MALAYSIAN JOURNAL OF MICROSCOPY

Journal homepage: https://malaysianjournalofmicroscopy.org

RESEARCH ARTICLE

ADSORPTION OF CHLORAMPHENICOL BY SAGO BARK-BASED ACTIVATED CARBON OPTIMIZED BY RESPONSE SURFACE METHODOLOGY

Siti Zawiyah Baharom, Erniza Mohd Johan Jaya, Ridzuan Zakaria, Mohd Azmier Ahmad*

School of Chemical Engineering, Engineering Campus, Universiti Sains Malaysia, 14300 Nibong Tebal, Pulau Pinang, Malaysia.

Abstract. When discharge into the environment, antibiotics like chloramphenicol (CAP), can pose significant environmental hazards, including harm to aquatic ecosystems. This pressing issue motivated the current study, which focuses on the development of sago bark-based activated carbon (SBAC) for the effective removal of CAP from water. SBAC was synthesized through a combined physicochemical activation approach involving chemical activation with potassium hydroxide (KOH) and subsequent microwave-assisted physical activation using carbon dioxide (CO_2) gas. The synthesis process was optimized using response surface methodology (RSM) with a central composite design (CCD). The optimal conditions were identified as a radiation power of 343.56 W, an activation time of 17.13 minutes, and a KOH impregnation ratio (IR) of 1.62 g/g. Under these optimized parameters, the SBAC achieved a CAP adsorption capacity of 68.87 mg/g and a production yield of 32.81%. The predictive models demonstrated high reliability, with actual results closely matching the predicted values, evidenced by low error rates of 2.41% for CAP uptake and 1.45% for yield. Structural analysis using scanning electron microscopy (SEM) highlighted a stark transformation in the material's morphology. The raw sago bark exhibited a dense, non-porous surface, whereas the activation process significantly enhanced its porosity, producing a highly porous SBAC surface. This confirmed the effectiveness of the combined activation techniques in creating a material with superior adsorption properties. The Brunauer-Emmett-Teller (BET) surface area of SBAC was 1003.23 m^2/g. Isotherm studies revealed that the adsorption of CAP onto SBAC adhered to the Freundlich model, indicative of multilayer adsorption on a heterogeneous surface. The material demonstrated an impressive maximum adsorption capacity, Q_m of 131.83 mg/g, showcasing its potential as an efficient adsorbent for mitigating antibiotic contamination in water.

Keywords: Adsorption, activated carbon, optimization, microwave, antibiotic.

Article Info

Received 6 January 2025
Accepted 23 April 2025
Published 2 June 2025

***Corresponding author: chazmier@usm.my**

ISSN: 1823-7010, eISSN: 2600-7444

1. INTRODUCTION

Chloramphenicol (CAP) is a broad-spectrum antibiotic widely used to treat bacterial infections in humans and animals. As a well-recognized chlorinated nitroaromatic compound, CAP plays an essential role in food production supply chains, particularly in livestock such as cattle, poultry, swine, and aquaculture species [1]. Aquatic environments can become polluted by CAP and its active metabolites excreted through urine and feces, originating from sources such as wastewater treatment plant effluents, hospital discharges, and agricultural runoff [2]. CAP has been widely banned in many countries, including the United States, Canada, China, and European Union member states, due to its harmful effects on human health. These adverse impacts include leukaemia, fatal aplastic anaemia, gray baby syndrome, and various blood disorders (EFSA CONTAM Panel 2014) [3]. Traditional wastewater treatment methods often fail to fully remove CAP, allowing it to persist in aquatic environments. Due to its persistence, the growth and reproduction of non-target organisms can be adversely affected, potentially disrupting aquatic ecosystems. Additionally, continuous exposure to residual CAP may accelerate the emergence of antibiotic-resistant bacteria among environmental microorganisms, posing a significant public health concern [4]. Adsorption is commonly used for the removal of pollutants, including antibiotics [4], heavy metal [5] and others. Adsorption is valued for its simplicity, high efficiency, and cost-effectiveness. Activated carbon (AC), a popular choice for this process, is traditionally sourced from coal, a non-renewable material associated with environmental concerns and high costs. Consequently, researchers are exploring the production of AC from agricultural by-products such as jackfruit peels [6] and coconut shell [7] as sustainable alternatives. In literature, the adsorption of CAP has been investigated using various adsorbents, including amino-functionalized silica, silica core-shell imprinted polymer [3], bamboo-based biochar, chemically treated bamboo-based charcoal, and commercial AC (F-300, ROW 08 Supra, and WG-12) [8]. However, these materials exhibit relatively low CAP adsorption capacities (Q_m) of below 100 mg/g.

Given the numerous parameters influencing optimal performance, enhancing AC production has become a key focus of recent research. Response Surface Methodology (RSM) is a statistical approach commonly used for efficient multivariable optimization and process modelling [9]. A commonly preferred method in Response Surface Methodology (RSM) is the Central Composite Design (CCD). This approach effectively builds predictive mathematical models that link input variables to corresponding responses while reducing the number of experimental trials needed. It also facilitates a comprehensive examination of interaction effects among the variables. Additionally, three-dimensional (3D) plots are utilized to visualize the influence of parameters, and Analysis of Variance (ANOVA) is employed to confirm the accuracy and significance of the results [10]. Microwave irradiation offers several advantages over conventional pyrolysis, including faster and more uniform heating, reduced processing time, and improved energy efficiency due to direct internal energy transfer. Additionally, microwave heating enables better temperature control, resulting in higher product yields and enhanced material properties. It also minimizes energy loss, reduces greenhouse gas emissions, and allows for selective heating, which can enhance the activation process and pore formation in AC [11]. The objective of this study was to synthesize AC from sago bark (SBAC) using a microwave activation method to effectively remove CAP from aqueous solutions, followed by optimization through RSM. The sago tree (*Metroxylon sago*), widely recognized for its production of sago flour, is considered an important crop in several countries, including Malaysia, Indonesia, the Philippines, and New Guinea [12]. With an estimated annual yield of 20 kilotons in Malaysia, sago bark is an abundant agricultural residue that offers a sustainable and environmentally friendly alternative [13].

2. MATERIALS AND METHODS

2.1 Materials and SBAC Preparation

The raw material used was sago bark, sourced from Mukah, Sarawak, Malaysia. Hydrochloric acid (HCl, 37% assay) and potassium hydroxide (KOH pellets, 85% purity) were procured from Sigma-Aldrich. MOX Gases Berhad, Malaysia, supplied high-purity carbon dioxide (CO_2) and nitrogen (N_2)

gases with a purity level of 99.99%. The sago bark precursor was thoroughly rinsed with distilled water and oven-dried at 60 °C for approximately 48 hours. It was then carbonized at 550 °C for 1.5 hours under a continuous flow of N_2 gas at 150 cm³/min, yielding the char material. To prevent oxidation and preserve its unique characteristics, the char was cooled under an inert flow of N_2 gas after carbonization. Following the cooling process, the char was impregnated with KOH for 24 hours at an impregnation ratio (IR) ranging from 0.5 to 2.0 g/g. The IR was calculated by dividing the weight of KOH (W_{KOH}) by the weight of char (W_{Char}) as follows:

$$Impregnation\ ratio\ (IR) = \frac{W_{KOH}}{W_{char}} \quad (1)$$

The impregnated samples were then dried and activated in a microwave oven for durations of 2 to 20 minutes, at power levels between 264 and 616 W. A constant flow of CO_2 gas at 150 cm³/min was maintained throughout the activation process [6,14].

2.2 Optimization Investigation

The dataset was processed using Design Expert software (version 12, STAT-EASE Inc., Minneapolis, USA) for optimization. The study employed Response Surface Methodology (RSM) with a Central Composite Design (CCD) to investigate the effects of three independent variables: radiation power (X_1), radiation duration (X_2), and impregnation ratio (IR, X_3). The two main responses analysed were the CAP uptake (Y_1) and the yield of SBAC (Y_2). The levels +1, 0, and -1 were used to define the experimental ranges for the variables. These levels corresponded to radiation power settings of 264, 440, and 616 W; durations of 2, 11, and 20 minutes; and IR of 0.50, 1.25, and 2.0 g/g, respectively. The yield of SBAC was calculated by dividing the weight of SBAC (W_{SBAC}) by the weight of the precursor ($W_{precursor}$) and multiplying by 100%, as follows:

$$Yield\ (\%) = \frac{W_{SBAC}}{W_{precursor}} \times 100\% \quad (2)$$

2.3 Characterization Methods

The study meticulously assessed the physicochemical properties of the materials, including surface area (determined by BET analysis), mesoporous characteristics, pore size distribution, and total pore volume. These analyses were conducted using a Micromeritics ASAP 2010 volumetric adsorption analyser. Elemental composition was determined using a PerkinElmer Series II 2400 analyser (USA). Additionally, surface morphology was examined through scanning electron microscopy (SEM) using a Quanta 450 FEG microscope (Netherlands), capturing detailed structural features.

2.4 Isotherm Investigation

Six different initial concentrations of CAP (C_o, mg/L) were prepared in Erlenmeyer flasks for the isotherm study: 10, 20, 40, 60, 80, and 100 mg/L. These flasks were placed in a water bath shaker set at 80 rpm. The temperature (30 °C), the mass of optimized SBAC, W_{SBAC} (0.20 g), and the solution volume, V (200 mL) were kept constant throughout the experiment. The residual concentration of CAP in the solution at equilibrium (C_e, mg/L) was measured using a UV-Vis spectrophotometer (Agilent Cary 60, USA). The amount of CAP adsorbed at equilibrium (q_e, mg/g) was then calculated using the following formula [4]:

$$q_e = \frac{(C_o - C_e)V}{W_{SBAC}} \quad (3)$$

Three adsorption isotherm models—Langmuir, Freundlich, and Temkin—were used to analyse the experimental results. Below are the related equations for each model [14,15]:

Langmuir:

$$q_e = \frac{Q_m K_L C_e}{1 + K_L C_e} \tag{4}$$

Freundlich:

$$q_e = K_F C_e^{1/n_F} \tag{5}$$

Temkin:

$$q_e = \frac{RT}{B} \ln(AC_e) \tag{6}$$

where K_L is the Langmuir constant associated with the adsorption strength (mg/g), and Q_m is the maximum adsorption capacity based on the Langmuir model (mg/g) in these equations. The level of surface heterogeneity is indicated by n_F (dimensionless), whereas K_F stands for the Freundlich constant ((mg/g)(L/mg)$^{1/n}$). The Temkin model constants for the adsorption energy and heat of adsorption are denoted by the parameters A and B, respectively.

3. RESULTS AND DISCUSSION

3.1 Optimization Process

3.1.1 Regression Models Development

The complete experimental design framework for synthesizing the enhanced SBAC showed variations in CAP adsorption capacity, which spanned from 39.63 to 93.22 mg/g and the SBAC yield, which ranged from 13.22% to 38.96%, as shown in Table 1. These variations underscore the effectiveness of the synthesis process in tailoring the properties of SBAC for optimal performance. To achieve reliable predictions of these outcomes, quadratic models were suggested by the software, using coded variables that effectively captured the relationships between input parameters and response variables, given below:

CAP uptakes (%), Y_1

$$Y_1 = 64.33 + 9.28X_1 + 8.68X_2 + 9.00X_3 + 2.80X_1X_2 - 0.1575X_1X_3 + 3.57X_2X_3 - 1.78X_1^2 + 0.9186X_2^2 - 3.46X_3^2 \tag{7}$$

SBAC yield (%), Y_2

$$Y_2 = 33.80 - 5.92X_1 - 5.12X_2 + 1.63X_3 - 2.00X_1X_2 - 0.5750X_1X_3 - 1.07X_2X_3 + 1.08X_1^2 - 1.66X_2^2 - 6.69X_3^2 \tag{8}$$

Table 1: Experimental runs for SBAC preparation

Run	Variables			Responses	
	Radiation power, X_1 (watt)	Radiation time, X_2 (minute)	IR, X_3 (g/g)	CAP uptake, Y_{CAP} (mg/g)	SBAC yield, Y_{yield} (%)
1	264 (-1)	2 (-1)	0.50 (-1)	39.63	33.12
2	616 (+1)	2 (-1)	0.50 (-1)	51.77	25.64
3	264 (-1)	20 (+1)	0.50 (-1)	45.17	28.96
4	616 (+1)	20 (+1)	0.50 (-1)	68.42	13.96
5	264 (-1)	2 (-1)	2.00 (+1)	70.52	30.99
6	616 (+1)	2 (-1)	2.00 (+1)	62.21	29.65
7	264 (-1)	2 (-1)	2.00 (+1)	50.78	38.96
8	616 (+1)	20 (+1)	2.00 (+1)	93.22	13.22
9	264 (-1)	11 (0)	1.25 (0)	50.12	38.59
10	616 (+1)	11 (0)	1.25 (0)	73.42	28.96
11	440 (0)	2 (-1)	1.25 (0)	57.52	36.52
12	440 (0)	20 (+1)	1.25 (0)	71.41	25.54
13	440 (0)	11 (0)	0.50 (-1)	50.96	23.44
14	440 (0)	11 (0)	2.00 (+1)	69.22	28.55
15	440 (0)	11 (0)	1.25 (0)	61.22	33.25
16	440 (0)	11 (0)	1.25 (0)	63.45	33.98
17	440 (0)	11 (0)	1.25 (0)	64.54	34.27
18	440 (0)	11 (0)	1.25 (0)	65.11	34.85
19	440 (0)	11 (0)	1.25 (0)	66.27	35.19
20	440 (0)	11 (0)	1.25 (0)	68.55	35.74

Figures 1(a) and (b) display the regression plots comparing the predicted values with the actual values for CAP uptake and SBAC yield, respectively. The statistical analysis reveals high coefficients of determination (R^2) and adjusted R^2 (adj-R^2), measured at 0.9787 and 0.9595 for CAP uptake, and 0.9781 and 0.9583 for SBAC yield. These values indicate that the regression models provide an excellent fit to the experimental data, capturing a significant portion of the variability in the dependent variables. Moreover, the standard deviations (SD) associated with the models were notably low, calculated as 2.41 for CAP uptake and 1.45 for SBAC yield, which signifies high precision and minimal prediction error. The low SD highlights the robustness of the models in replicating experimental results with minimal deviations. The models' reliability is further supported by the adequate precision (AP) values, which were 31.59 for CAP uptake and 26.65 for SBAC yield. These AP values far exceed the recommended minimum threshold of 4, underscoring the models' strong signal-to-noise ratio. This robust ratio confirms the ability of the models to reliably predict the responses within the tested experimental range, ensuring their validity and applicability for further optimization studies [16].

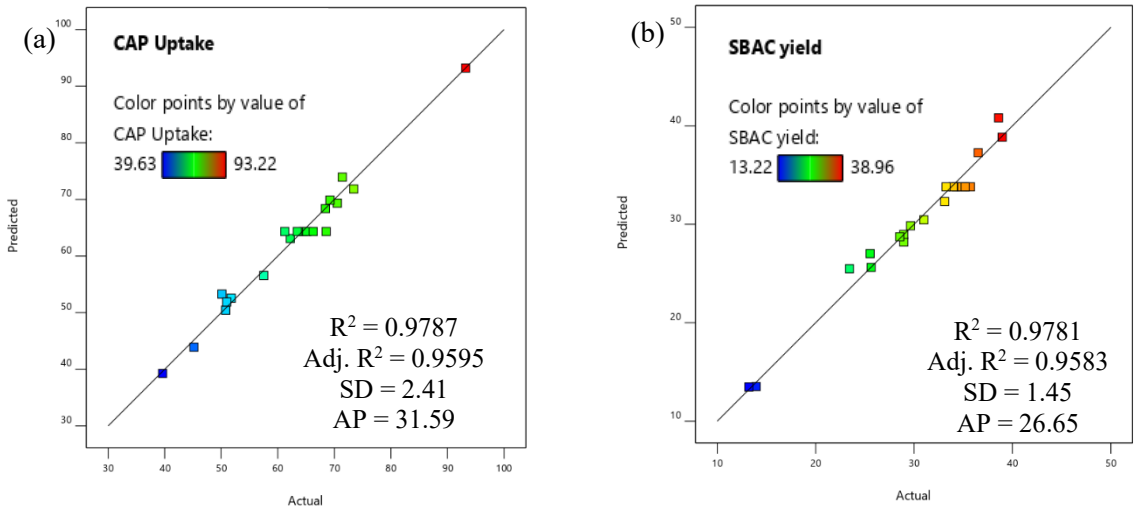

Figure 1: Plots of predicted versus actual values for (a) CAP update and (b) SBAC yield

3.1.2 Analysis of Variance (ANOVA)

Table 2 presents the results of the analysis of variance (ANOVA) for CAP uptake and SBAC yield, highlighting their statistical significance and contributing factors. Both responses exhibited p-values below 0.0001, confirming the models' overall significance [10]. For CAP uptake, the analysis identified the significant model terms as X_1, X_2, X_3, X_1X_2, X_2X_3, and X_3^2. In the case of SBAC yield, the significant terms included X_1, X_2, X_3, X_1X_2, and X_3^2, emphasizing the influence of linear, interactive and quadratic effects on the response. The F-values further clarify the contributions of these factors. For CAP uptake, the responses were nearly equally influenced by radiation power (F = 147.81), radiation time (F = 129.35), and IR (F = 138.96), indicating balanced contributions from these variables. In contrast, SBAC yield was predominantly affected by radiation power (F = 166.49) and radiation time (F = 124.67), with IR playing a comparatively smaller role. These findings underline the importance of optimizing linear, interactive and quadratic effects to achieve desired outcomes for CAP uptake and SBAC yield, demonstrating the robustness and reliability of the statistical models employed. The p-values for the lack-of-fit test in the ANOVA for CAP uptakes and SBAC yield responses were 0.5541 and 0.0692, respectively, indicating that the lack of fit was not statistically significant. This is desirable, as it suggests that the chosen model adequately represents the data without systematic deviations [17].

Table 2: ANOVA results for CAP uptakes and SBAC yield responses

Source	Response 1, Y_1: CAP uptakes by SBAC					Response 2, Y_2: SBAC yield				
	Sum of Squares	DF	Mean Square	F Value	p-value	Sum of Squares	DF	Mean Square	F Value	p-value
Model	2677.99	9	297.55	51.05	< 0.0001	938.90	9	104.32	49.58	< 0.0001
X_1	861.56	1	861.56	147.81	< 0.0001	350.35	1	350.35	166.49	< 0.0001
X_2	753.94	1	753.94	129.35	< 0.0001	262.35	1	262.35	124.67	< 0.0001
X_3	810.00	1	810.00	138.96	< 0.0001	26.41	1	26.41	12.55	0.0053
X_1X_2	62.61	1	62.61	10.74	0.0083	31.92	1	31.92	15.17	0.0030
X_1X_3	0.1984	1	0.1984	0.0340	0.8573	2.64	1	2.64	1.26	0.2884
X_2X_3	101.96	1	101.96	17.49	0.0019	9.16	1	9.16	4.35	0.0635
X_1^2	8.68	1	8.68	1.49	0.2504	3.24	1	3.24	1.54	0.2432
X_2^2	2.32	1	2.32	0.3981	0.5422	7.58	1	7.58	3.60	0.0870
X_3^2	32.85	1	32.85	5.64	0.0390	123.26	1	123.26	58.58	< 0.0001
Lack of fit	27.28	5	5.46	0.8799	0.5541	17.03	5	3.41	4.25	0.0692

3.1.3 Three-dimensional (3D) Surface Plot

Figure 2(a) displays a three-dimensional (3D) surface plot illustrating the combined effects of radiation power and impregnation ratio (IR) on CAP uptake, while Figure 2(b) depicts a 3D surface plot showing the influence of radiation power and radiation time on SBAC yield. In Figure 2(a), the maximum CAP uptake of 93.22 mg/g was achieved at the highest radiation power of 616 W and an IR of 2.00 g/g, demonstrating the significant positive impact of these parameters. The plot reveals that as radiation power increased from 264 to 616 W, CAP uptake exhibited a marked rise, particularly within the IR range of 1.00 to 2.00 g/g. This trend highlights the synergistic interaction between radiation power and IR in enhancing CAP adsorption. The improvement in CAP uptake can be attributed to the increased radiation power, which facilitates more effective heating. This process accelerates the removal of volatile substances from the material, thereby creating additional pores and significantly enhancing the surface area. These structural changes improve the adsorption capacity of SBAC, making it more efficient in capturing CAP molecules. This analysis underscores the critical role of optimizing radiation power and IR to maximize the adsorption performance of SBAC [18]. Likewise, a higher IR led to a greater concentration of K^+ ions, which facilitated deeper penetration into the material's matrix. This enhanced ion interaction promoted more extensive pore development within the structure, resulting in improved porosity and surface characteristics [19].

Figure 2(b) illustrates the relationship between radiation power and radiation time on SBAC yield, highlighting that the minimum yield of 13.22% was recorded at the highest radiation power of 616 W and the longest radiation time of 20 minutes. This observation underscores the adverse impact of prolonged exposure to high radiation power and time on the material's yield. As the radiation time extended from 11 to 20 minutes, a progressive decline in SBAC yield became more pronounced, especially at elevated radiation power levels ranging from 440 to 616 W. The combined effect of increased radiation power and extended exposure time intensified the thermal cracking process. This process, while potentially beneficial for enhancing porosity, compromises the overall material retention, leading to lower yields. These findings emphasize the importance of optimizing radiation parameters to balance the trade-off between enhancing adsorption performance and maintaining a satisfactory yield of SBAC.

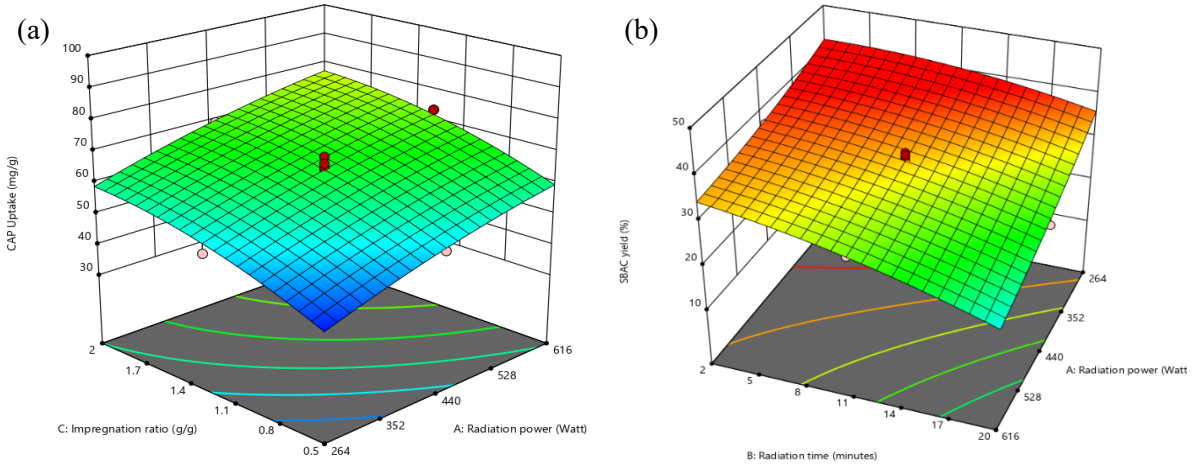

Figure 2: 3D surface plots for (a) CAP uptakes and (b) SBAC yield

The optimal conditions for the process variables and target responses were identified by minimizing the input variables while maximizing the desired outcomes. Through RSM, the ideal parameters were determined to be 343.56 W for radiation power, 17.13 minutes for radiation time, and 1.62 g/g for the IR. Under these conditions, the predicted optimum responses were 68.87 mg/g for CAP uptake and 32.81% for SBAC yield. Experimental validation of these optimized conditions yielded actual response values of 70.10 mg/g for CAP uptake and 33.46% for SBAC yield. The discrepancies between the predicted and actual values corresponded to low error percentages of 1.75% and 1.94%, respectively. These minimal deviations highlight the high accuracy of the developed models in predicting the responses.

3.2 Characteristics of Samples

3.2.1 Surface Area and Pores Characteristic

Table 3 shows the surface area and pore characteristics for the samples. The precursor exhibited minimal porosity, with a BET surface area of only 2.11 m^2/g and an almost negligible total pore volume of 0.0001 cm^3/g. Additionally, no mesopore surface area or average pore diameter could be detected in the precursor. Following carbonization and activation, the optimized SBAC displayed remarkable improvements. The BET surface area increased dramatically to 1003.23 m^2/g, accompanied by a mesopore surface area of 725.33 m^2/g and a total pore volume of 0.3326 cm^3/g. The average pore diameter also showed a significant rise, from 2.24 nm in the char to 2.76 nm in the SBAC. This enhancement can be attributed to the synergistic effects of KOH chemical activation and CO_2 gasification. KOH treatment played a crucial role in expanding the pore network, while the bombardment of CO_2 gas further refined the pore structure and enhanced the overall surface area. Such an improvement in porosity and surface properties aligns with previous studies, such as those involving teak wood-based AC, where the combined use of KOH and CO_2 effectively increased the pore size from 2.64 nm to 2.97 nm. These results underscore the efficacy of KOH/CO_2 activation in developing well-

structured porous materials and enhanced adsorptivity [20]. Moreover, the unique texture of sago bark, which is firm but not excessively hard, allows for efficient activation, leading to a significant increase in BET surface area, mesopore surface area, and total pore volume, making SBAC an excellent choice for adsorption applications. Therefore, choosing SBAC was a good decision from the start.

Table 3: Surface area and pore characteristics of samples

Samples	BET surface area (m^2/g)	Mesopores surface area (m^2/g)	Total pore volume (cm^3/g)	Average pore diameter (nm)
Precursor	2.11	-	0.0001	-
Char	489.63	318.86	0.2146	2.24
SBAC	1003.23	725.33	0.3326	2.76

3.2.2 SEM Images

Figure 3 illustrates the scanning electron microscopy (SEM) images, showcasing the surface morphology of the samples. In Figure 3(a), the precursor's surface is observed to be compact, dense, and devoid of any distinguishable pores. This appearance aligns with the structural composition of lignocellulosic materials, predominantly containing lignin, cellulose, hemicellulose, and residual tar, which inhibit the formation of a porous structure at this stage [17]. The compact nature reflects the unprocessed state of the material prior to carbonization and activation. In stark contrast, Figure 3(b) highlights the dramatic transformation observed in the optimized SBAC. The surface of the SBAC is highly porous, characterized by an abundance of visible empty cavities. This significant change is attributed to the thermal and chemical processes employed during its synthesis. Initially, the precursor underwent carbonization, during which moisture, volatile organic compounds, and other light elements evaporated and escaped, leaving behind a rudimentary porous framework [20]. The subsequent activation process further enhanced this structure. Chemical activation with KOH played a critical role by infiltrating the material and reacting with the carbon matrix, expanding existing pores and creating new ones. This was followed by CO_2 gasification, where the interaction of CO_2 with the material's surface intensified the pore development by etching away weaker carbon bonds and removing residual impurities [10].

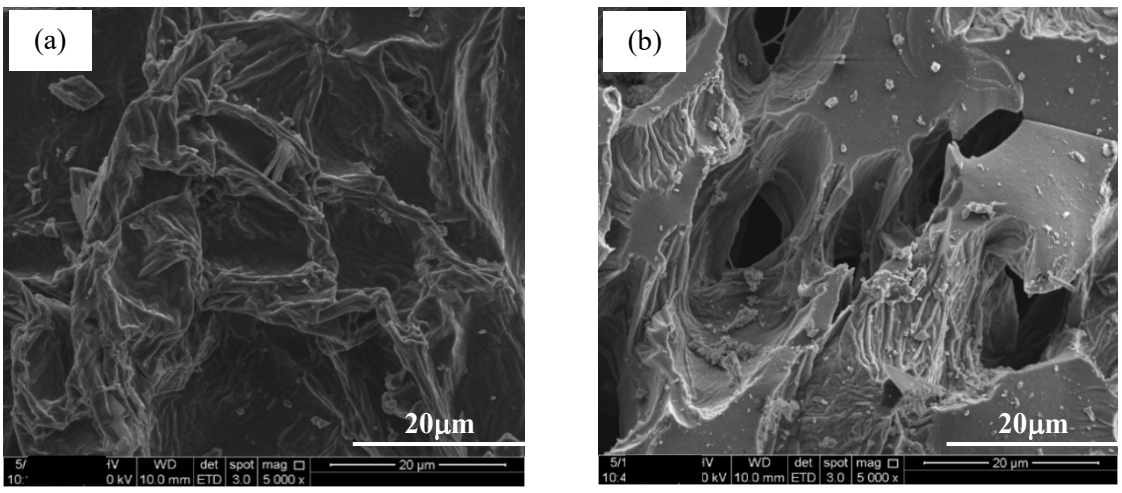

Figure 3: SEM images of (a) sago bark and (b) SBAC

3.3 Adsorption Isotherm

Figure 4 shows the isotherm plots and Table 4 shows the summary of isotherm parameters for AMOX-SBAC system at 30 °C. Among the tested models, the Freundlich isotherm provided the most accurate representation of CAP adsorption onto the SBAC. This conclusion is supported by its lowest RMSE value of 1.19 and an error percentage of 4.40%, indicating a high degree of reliability in predicting the adsorption behaviour. The Freundlich model describes adsorption as a multilayer process occurring on a heterogeneous surface, which is consistent with the observed data. The heterogeneity factor, n_F, calculated from the model, was found to lie between 1 and 10, which is 1.51, confirming that the adsorption process was favourable. This range suggests that the SBAC surface possesses active sites with varying affinities for CAP molecules, promoting efficient adsorption across a diverse set of interactions [4]. The Q_m value reached 131.83 mg/g, demonstrating the material's ability to adsorb CAP effectively. This Q_m value was significantly higher than that of CAP adsorption by amino-functionalized silica (29.60 mg/g), silica core-shell imprinted polymer (32.26 mg/g) [3], bamboo-based biochar (8.46 mg/g), chemically treated bamboo-based charcoal (2.35 mg/g), and commercial AC – F-300 (0.10 mg/g), ROW 08 Supra (0.12 mg/g), and WG-12 (0.11 mg/g) [8] – demonstrating the superiority of SBAC over other adsorbents in removing CAP.

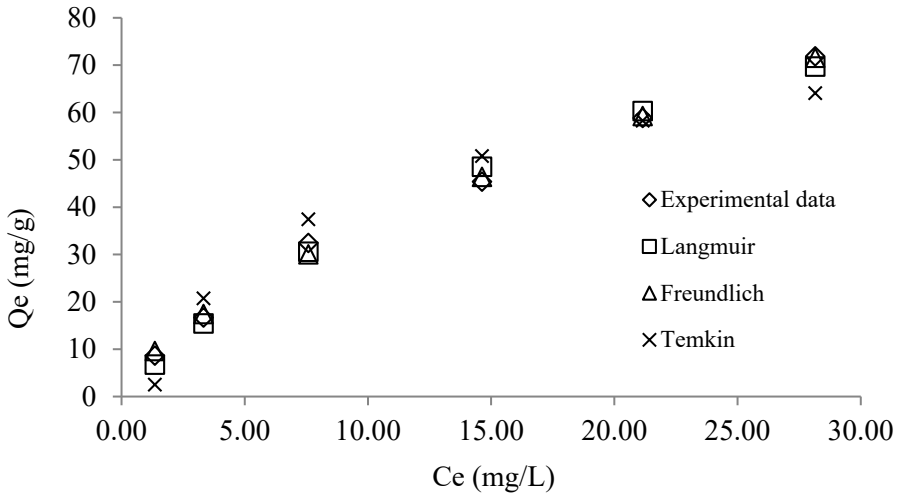

Figure 4: Isotherm plots representing CAP-SBAC adsorption system at 30 °C

Table 4: Isotherm parameters for CAP-SBAC system at 30 °C

Isotherm models	Parameters	CAP-SBAC
Langmuir	Q_m (mg/g)	131.83
	K_L (L/mg)	0.04
	RMSE	2.05
	Error (%)	7.92
Freundlich	n_F	1.51
	K_F (mg/g)(L/mg)$^{1/n}$	7.86
	$1/n_F$	0.66
	RMSE	1.19
	Error (%)	4.40
Temkin	A_T (L/mg)	0.83
	B_T (L/mg)	20.30
	RMSE	5.32
	Error (%)	22.44

4. CONCLUSIONS

SBAC was effectively synthesized under the optimal conditions identified using response surface methodology (RSM), which included a radiation power of 343.56 W, an activation time of 17.13 minutes, and an impregnation ratio (IR) of 1.62 g/g. These conditions yielded an SBAC with a CAP adsorption capacity of 68.87 mg/g and a production yield of 32.81%. Regression analysis reinforced the model's robustness, exhibiting high R^2 of 0.9787 for CAP adsorption and 0.9781 for SBAC yield. Furthermore, the models displayed low SD of 2.41 and 1.45 for CAP uptake and yield, respectively, alongside high AP values of 31.59 and 26.65, underscoring the predictive strength and precision of the optimization framework. ANOVA revealed that CAP uptake was equally influenced by radiation power, activation time, and IR, while the SBAC yield was predominantly affected by radiation power and activation time. Characterization of the optimized SBAC demonstrated exceptional properties, including a BET surface area of 1003.23 m^2/g, a mesopore surface area of 725.33 m^2/g, a total pore volume of 0.3326 cm^3/g, and an average pore diameter of 2.76 nm, confirming its mesoporous nature. SEM analysis further validated the successful activation process, revealing a well-developed porous structure that enhances its adsorption capacity. The adsorption behaviour of CAP onto the optimized SBAC was best described by the Freundlich isotherm model, with Q_m of 131.83 mg/g.

Acknowledgements

This research is supported by Malaysian Ministry of Higher Education under the Fundamental Research Grant Scheme (project code: FRGS/1/2023/TK05/USM/02/8).

Author Contributions

All authors contributed toward data analysis, drafting and critically revising the paper and agree to be accountable for all aspects of the work.

Disclosure of Conflict of Interest

The authors have no disclosures to declare.

Compliance with Ethical Standards

The work adheres to ethical standards, ensuring that all experimental procedures and methodologies were conducted with integrity and respect for ethical guidelines.

References

[1] Karikalan, N., Yamuna, A. & Lee, T. Y. (2023). Ultrasensitive detection of ineradicable and harmful antibiotic chloramphenicol residue in soil, water, and food samples. *Analytica Chimica Acta,* 1243, 340841.

[2] Khan, A. H., Aziz, H. A., Palaniandy, P., Naushad, M., Cevik, E. & Zahmatkesh, S. (2023). Pharmaceutical residues in the ecosystem: Antibiotic resistance, health impacts, and removal techniques. *Chemosphere,* 339, 139647.

[3] Idris, Z. M., Hameed, B. H., Ye, L., Hajizadeh, S., Mattiasson, B. & Din, A. T. M. (2020). Amino-functionalised silica-grafted molecularly imprinted polymers for chloramphenicol adsorption. *Journal of Environmental Chemical Engineering,* 8(5), 103981.

[4] Mohamad, F. M. Y., Abdullah, A. Z. & Ahmad, M. A. (2024). Amoxicillin adsorption from aqueous solution by Cu(II) modified lemon peel based activated carbon: Mass transfer simulation, surface area prediction and F-test on isotherm and kinetic models. *Powder Technology,* 438(29), 119589.

[5] Khan, M. N. N., Zainol, M. R. R. M. A., Mohamad, F. M. Y. & Ahmad, M. A. (2024). Turning waste into wonder: Arsenic removal using rice husk based activated carbon. *Journal of Engineering Research,* In Press, 1-14.

[6] Mohamad, F. M. Y., Abdullah, A. Z. & Ahmad, M. A. (2023). Adsorption of remazol brilliant blue R dye onto jackfruit peel based activated carbon: Optimization and simulation for mass transfer and surface area prediction. *Inorganic Chemistry Communications,* 158(9), 111721.

[7] Yusop, M. F. M., Jaya, E. M. J., Din, A. T. M., Bello, O. S. & Ahmad, M. A. (2022). Single-stage optimized microwave-induced activated carbon from coconut shell for cadmium adsorption. *Chemical Engineering & Technology,* 45(11), 1943-1951.

[8] Nguyen, L. M., Nguyen, N. T. T., Nguyen, T. T. T., Nguyen, T. T., Nguyen, D. T. C. & Tran, T. V. (2022). Occurrence, toxicity and adsorptive removal of the chloramphenicol antibiotic in water: a review. *Environmental Chemistry Letters,* 20(3), 1929-1963.

[9] Daouda, M. M. A., Akowanou, A. V. O., Mahunon, S. E. R., Adjinda, C. K., Aina, M. P. & Drogui, P. (2021). Optimal removal of diclofenac and amoxicillin by activated carbon prepared from coconut shell through response surface methodology. *South African Journal of Chemical Engineering,* 38(1), 78-89.

[10] Firdaus, M. Y. M., Azan, M. T. J., Iylia, I., Zuhairi, A. A. & Azmier, M. A. (2023). Optimization and mass transfer simulation of remazol brilliant blue R dye adsorption onto meranti wood based activated carbon. *Arabian Journal of Chemistry,* 16(5), 104683.

[11] Qi, G., Pan, Z., Zhang, X., Chang, S., Wang, H., Wang, M., Xiang, W. & Gao, B. (2023). Microwave biochar produced with activated carbon catalyst: Characterization and adsorption of heavy metals. *Environmental Research,* 216, 114732.

[12] Siruru, H., Syafii, W., Wistara, N. & Pari, G. (2019). Characteristics of sago pith and sago bark waste from Seram Island, Maluku, Indonesia. *Biodiversitas Journal of Biological Diversity,* 20(12), 3517-3526.

[13] M. Amin, N., Sabli, N., Izhar, S. & Yoshida, H. (2019). A review: Sago wastes and its applications. *Pertanika Journal of Science and Technology,* 27, 1841-1862.

[14] Mohamad, F. M. Y., Abdullah, A. Z. & Ahmad, M. A. (2023). Malachite green dye adsorption by jackfruit based activated carbon: Optimization, mass transfer simulation and surface area prediction. *Diamond and Related Materials,* 136(9), 109991.

[15] Yusop, M. F. M., Ahmad, M. A., Rosli, N. A., Gonawan, F. N. & Abdullah, S. J. (2021). Scavenging malachite green dye from aqueous solution using durian peel based activated carbon. *Malaysian Journal of Fundamental and Applied Sciences,* 17(1), 95-103.

[16] Beyan, S. M., Prabhu, S. V., Sissay, T. T. & Getahun, A. A. (2021). Sugarcane bagasse based activated carbon preparation and its adsorption efficacy on removal of BOD and COD from textile effluents: RSM based modeling, optimization and kinetic aspects. *Bioresource Technology Reports,* 14, 100664.

[17] Firdaus, M. Y. M., Azrina, A. & Azmier, M. A. (2022). Conversion of teak wood waste into microwave-irradiated activated carbon for cationic methylene blue dye removal: Optimization and batch studies. *Arabian Journal of Chemistry,* 15(9), 104081.

[18] Mahari, W. A. W., Zainuddin, N. F., Nik, W. M. N. W., Chong, C. T. & Lam, S. S. (2016). Pyrolysis Recovery of Waste Shipping Oil Using Microwave Heating. *Energies,* 9(10), 780.

[19] Durán-Jiménez, G., Rodriguez, J., Stevens, L., Kostas, E. T. & Dodds, C. (2024). Microwave pyrolysis of waste biomass and synthesis of micro-mesoporous activated carbons: The role of textural properties for CO2 and textile dye adsorption. *Chemical Engineering Journal,* 488, 150926.

[20] Firdaus, M. Y. M., Nasran, M. N. K., Ridzuan, Z., Zuhairi, A. A. & Azmier, M. A. (2023). Mass transfer simulation on remazol brilliant blue R dye adsorption by optimized teak wood Based activated carbon. *Arabian Journal of Chemistry,* 16(6), 104780.